An Analysis of the Dynamic Light Scattering Spectra of Wormlike Chains: β-Connectin from Striated Muscle

S. Fujime* and H. Higuchi[1]

Graduate School of Integrated Science, Yokohama City University, 22-2 Seto, Kanazawa, Yokohama 236, Japan

*Received April 22, 1993; Revised Manuscript Received August 3, 1993**

ABSTRACT: Connectin (titin) is a large filamentous protein (single peptide) with a molecular mass of ~3 MDa, a contour length (L) of ~900 nm, and a diameter of ~4 nm and resides in striated muscle. Electron microscopy reveals that isolated connectin assumes a Gaussian coil. This paper describes in some detail the analysis of the dynamic light scattering (DLS) spectra for isolated connectin filaments in solution in terms of a wormlike chain model with a preaveraged hydrodynamic interaction. The analysis gives the translational diffusion coefficient $D = 3.60 \times 10^{-8}$ cm^2/s at 10 °C, the mean-square end-to-end distance $\langle R^2 \rangle = (163\ \text{nm})^2$, and the number $\gamma L = 30$ and length $\gamma^{-1} = 30$ nm of the Kuhn statistical segments. These results give the ratio $R_g/R_s = 1.51$, which is characteristic of Gaussian coils, and the spatial ranges $0.5 \leq KR_g \leq 2$ and $0.2 \leq K/\gamma \leq 1$, where R_g is the radius of gyration and R_s is the Stokes radius. In such spatial ranges as the present ones, the numerical method described here may be the simplest of the available numerical methods to analyze of those feasible for the analysis of the DLS spectra. Possible effects of sample polydispersity on the analysis are also examined.

Introduction

Connectin (also called titin) is a large filamentous protein (single peptide) with a molecular mass of ~3 MDa, a length of ~900 nm, and a diameter of ~4 nm and resides in a striated muscle (for reviews, see refs 2 and 3). Among muscle filaments, a thin filament is semiflexible and a thick filament is rigid. On the other hand, electron microscopy shows that the isolated connectin molecule assumes a Gaussian coil (see, for example, Figure 5c of ref 4). However, few studies have been reported on the physical properties of isolated connectin. We have studied some aspects of the physical properties of connectin by means of dynamic light scattering (DLS) spectroscopy.[5] In the course of that study, it turned out that connectin molecules were a good example for application of DLS spectroscopy to the study of biological supramolecules with a Gaussian-coil nature.[6]

Although DLS spectroscopy has been widely used in characterizing Gaussian coils in solution in the field of polymer physics and chemistry, few applications have been made for biological supramolecules with a Gaussian-coil nature. As an example of the latter, in the present paper the analysis of DLS spectra of isolated connectin is discussed in light of a crude theoretical model for a wormlike chain with a preaveraged hydrodynamic interaction.

The usual "bead-and-spring" model of Rouse and Zimm for a Gaussian coil (or flexible chain) consists of N Gaussian segments, each of average length b, connecting $N + 1$ identical beads.[7] The segments are assumed to provide Hookean restoring forces to the beads. The contour length of the coil is given by $L = Nb$, and its mean-square end-to-end distance is given by $\langle R^2 \rangle = Nb^2 = Lb$. Another model, the so-called "wormlike chain" model of Kratky and Porod,[7] considers a continuous space curve with a contour length L and a Kuhn statistical segment length γ^{-1}. For the wormlike chain, $\langle R^2 \rangle$ is given by

$$\langle R^2 \rangle = 2L^2[\exp(-2\gamma L) - 1 + 2\gamma L]/(2\gamma L)^2 \qquad (1)$$

Equation 1 becomes $\langle R^2 \rangle = L/\gamma$ for $\gamma L \gg 1$, so that γ^{-1} and γL in the wormlike chain model for large γL correspond, respectively, to b and N in the bead-and-spring model. The Kirkwood formula for the translational diffusion coefficient, D, of Gaussian coils is given by[7]

$$D = (k_B T/3\pi\eta L)[1 + 1.84(\gamma L)^{1/2}] \qquad (2)$$

where k_B is the Boltzmann constant, T is the absolute temperature, η is the solvent viscosity, and the factor 1.84 comes from $(\zeta/6\pi\eta)(6/\pi)^{1/2}(8/3)$ for $(\zeta/6\pi\eta) = 1/2$ (the "segment number" in the original Kirkwood expression has been replaced with γL in eq 2 for our continuous chain model). The familiar Debye result of the scattering function for Gaussian coils is given by[7]

$$P(x) = (2/x^2)[\exp(-x) - 1 + x] \qquad (3)$$

$$x = K^2\langle R^2 \rangle/6 \qquad (4)$$

where K is the length of the scattering vector, $K = (4\pi/\lambda)\sin(\theta/2)$ (λ = the wavelength of light in the medium; θ = the scattering angle).

The intensity autocorrelation function of the scattered light is given by $G^2(t) = B\{\beta[g^1(t)]^2 + 1\}$, where $t = mt_s$ ($m = 1, 2, ..., 256$; t_s = the sampling time), B is the baseline level, β is a constant, and $g^1(t)$ is the normalized field correlation function. The expansion method can be used to obtain the average decay rate $\bar{\Gamma}$; $g^1(t) = (1 + m_2t^2 - m_3t^3)\exp(-\bar{\Gamma}t)$. The quantity $\bar{\Gamma}/K^2$ is called an apparent diffusion coefficient, D_{app}.

Summary of Experimental Results

In the following, we first summarize the experimental results for connectin to be detailed elsewhere.[5]

An ($8 \times N$)-bit digital correlator (K7032CE, Malvern Instruments, Malvern, U.K.) was used to measure $G^2(t)$ for a 488-nm beam from an Ar^+ ion laser (Model 95, Lexel Corp., Palo Alto, CA). The temperature of the scattering sample was kept at 10.0 ± 0.1 °C. Throughout this paper, we express D and D_{app} (and any difference from and between them) in units of 10^{-8} cm^2/s. We also express K in units of 10^5 cm^{-1} and $\langle R^2 \rangle$ in eq 1 in units of 10^{-10} cm^2. Connectin preparations used were in a partially (*in situ*) proteolized form, called β-connectin (titin 2).[2] Unless otherwise stated, therefore, connectin means β-connectin throughout this paper.

* Abstract published in *Advance ACS Abstracts*, October 15, 1993.

0024-9297/93/2226-6261$04.00/0

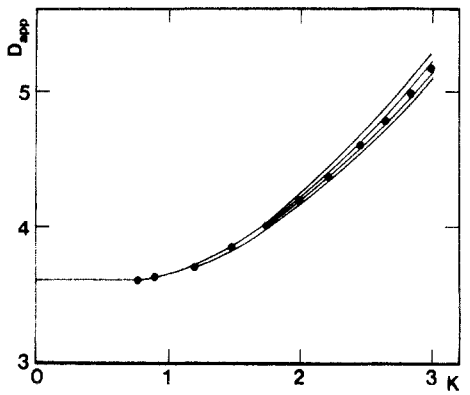

Figure 1. D_{app} versus K relationships at 10 °C. Experimental data (filled circles) were taken from ref 5. Solid lines show simulated results; from top to bottom, $\langle R^2\rangle$ = 2.80, 2.70, 2.60, and 2.50 (and γL = 30).

Figure 1 shows the D_{app} versus K relationships for a 0.7 mg/mL connectin solution. (To emphasize the low-K behavior of D_{app}, we display D_{app} against K, instead of the conventional K^2, throughout this paper.) The dependence of D_{app} on protein concentrations (0.8–0.2 mg/mL) was weak, but a slight tendency was observed that a lower concentration gave a little larger D_{app}. It should be noted that the D_{app} at the lowest K (at the angle of 25°) was only very slightly smaller than that at the next lowest K (at 30°). From data in Figure 1, the D value of connectin, D_{app} at K = 0, was estimated to be 3.60. Equation 2 gave γL = 25 or $\langle R^2\rangle$ = 3.18 = (178 nm)^2 for D = 3.60 and L = 900 nm. Noting $\langle R^2\rangle \sim L/\gamma$ and $1.84(\gamma L)^{1/2} \gg 1$ for large γL, we can approximate eq 2 as $D \sim 1.84(k_B T/3\pi\eta)\langle R^2\rangle^{-1/2}$, which gives $\langle R^2\rangle$ = 2.63 = (162 nm)^2, or γL = 30 for L = 900 nm.

The K dependence of the static scattering intensity $I(K)$ would provide us with information about the mean-square radius of gyration, $\langle R_g^2\rangle$ ($=\langle R^2\rangle/6$ for Gaussian coils). Because of technical difficulties, our measurements were not carried out to sufficiently small K values. Thus, the observed I versus K relationship was simply compared with $k_s P(x)$, where k_s is the scale factor and $P(x)$ is given by eq 3. From this analysis, we obtain $\langle R^2\rangle$ = 2.60–2.70 = (160 nm)^2. Equation 1 gives γL = 30 for $\langle R^2\rangle$ = 2.66 = (163 nm)^2 and L = 900 nm. Following the method detailed below, the D_{app} versus K relationships were simulated for $\langle R^2\rangle$ values from 2.50 to 2.80, and the results are shown in Figure 1. The analysis of the contribution to D_{app} from internal modes of motion suggested again $\langle R^2\rangle$ = 2.60–2.70.

The D value of connectin was 3.60 (and 3.65 at infinite dilution) at 10 °C, which equaled 4.87 (4.94) at 20 °C in water. By assuming the specific volume of connectin to be v = 0.73 (a typical value for proteins), we obtained the molecular mass of connectin to be M = 3150–3100 kDa for the literature value of the sedimentation coefficient, s = 17 S at 20 °C in water.[8] The light scattering D value is of the z average over the size distribution, whereas the s value is of the weight average. If this fact is taken into account, the molecular mass of connectin is close to but a little smaller than 3.0 MDa. This value of molecular mass strongly supports our implicit assumption of molecular dispersion of connectin in solution.

Results and Discussion

1. Brief Summary of Theoretical Backgrounds. A theoretical formulation for the field correlation function, $g^1(t)$, of light scattered from a monodisperse solution of Gaussian coils was first described by Pecora.[9] For purposes of self-containment, we briefly summarize it in our own notations for a continuous chain model with a contour length L.[10-12] The formal expression of $g^1(t)$ is given by

$$g^1(t) = \exp(-DK^2t)S(K,t)/S(K,0) \quad (5)$$

$$S(K,t) = (1/L^2)\int\int J(s,s',t)\,ds\,ds' \quad (6)$$

where the integrations in eq 6 are carried out over (s and s') = $[-L/2, L/2]$. The explicit expression of $J(s,s',t)$ in the free-draining limit is given by

$$J(s,s',t) = \exp[-x\sum{}'(2/\pi^2n^2)\{Q(n,s)^2 + Q(n,s')^2 - 2Q(n,s)\,Q(n,s')\exp(-t/\tau_n)\}] \quad (7)$$

where x is given by eq 4 and Σ' stands for the summation over positive integers n. Explicit forms of various quantities in eq 7 are defined by

$$Q(n,s) = \sin(n\pi s/L) \quad \text{(for odd } n\text{)}$$
$$= \cos(n\pi s/L) \quad \text{(for even } n\text{)} \quad (8)$$

$$\tau_n = \langle R^2\rangle/(3\pi^2n^2D_{[n]}) \quad \text{(for } n = 1, 2, 3, \ldots\text{)} \quad (9)$$

$$D_{[n]} = (k_B T/\zeta L) \quad \text{(in the free-draining limit)} \quad (10)$$

where ζ is the friction coefficient per unit length of the chain. The double integration in eq 6 can be carried out analytically for t = 0, yielding the Debye result of the scattering function $P(x) = S(K,0)$ for Gaussian coils (see eq 3). The first time derivative of eq 5 at t = 0 gives

$$D_{app} = D + \sum{}'D_{[n]}a_n(x) \quad (11)$$

$$a_n(x) = 2I_n(x)\{x - 2x^2I_n(x)[1 - (-1)^n\exp(-x)]\}/P(x) \quad (12)$$

where $I_n(x) = [x^2 + (\pi n)^2]^{-1}$. (Also $a_n(x) = Lf(X,n,0)$, but $f(X,n,0)$ given by eq C9 of ref 12 is not as concise as eq 12.) Equation 11 will be discussed later. Briefly speaking, eq 11 describes that D_{app} for Gaussian coils increases with x and hence K. The excess of D_{app} over D comes from the contribution from the conformation fluctuations, the terms under the summation sign. For later purposes, the Kirkwood formula for D is cited again in the form (cf. eq 2)

$$D = D^\circ[1 + f_0] \quad (13)$$

where

$$D^\circ = (k_B T/3\pi\eta L) \quad (14)$$

$$f_0 = 3.685(\gamma L)^{1/2}\sigma \quad (15)$$

and $\sigma = (\zeta/6\pi\eta)$. [The factor 3.685 comes from $(6/\pi)^{1/2}\cdot(8/3)$.]

2. Numerical Methods. For the integration of eq 6, an adaptive quadrature subroutine (ADAPT) in multidimensions was used.[13] To save computation time, a trigonometric relation, $\Sigma'(2/\pi^2n^2)[Q(n,s)^2 + Q(n,s')^2] = {}^1/_6 + y^2 + y'^2$, was used in eq 7,[9] where $y = s/L$ and (y and y') = $[-{}^1/_2, {}^1/_2]$. Furthermore, symmetry considerations permitted us to reduce the integration ranges over y and y' to $[0, {}^1/_2]$. The relative error tolerance EPS = $\Delta S(K,t)/S(K,t)$ in the integration itself was first set to be 1×10^{-5}, and $E(n_{max}) = |S(K,0) - P(x)|/P(x)$ for the maximum mode number, n_{max}, in eq 7 was computed; when L = 900 nm and γL = 20–40, $E(n_{max}) \le$ EPS was observed for $n_{max} \ge$ 30 even at the highest scattering angle. Thus the computation of $g^1(t)$ was carried out for n_{max} = 30, EPS = 1×10^{-3}, scattering angles of 25° and 30–120° in steps of 10°, and t = 0 and 2^p (p = 0–8) in units of the sampling

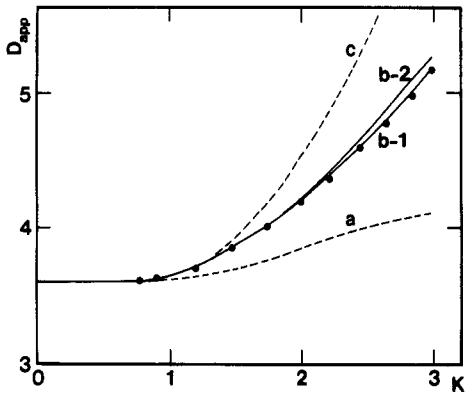

Figure 2. Simulated D_{app} versus K relationships at 10 °C. Simulations were made for L = 900 nm and γL = 30; free draining (label a), partial draining (labels b-1 and b-2), and a hypothetical situation (label c; see text). $D°$ in $D_{[n]}$ was put equal to D(obsd)/$(1 + f_0)$ in label b-1 and to $(k_BT/3\pi\eta L)$ in label b-2. Filled circles were taken from Figure 1.

time, t_s, at the experiment. From the table of computed results, $G^2(t) = 1 + [g^1(t)]^2$ was constructed for $t = mt_s$ (m = 1, 2, 3, ..., 256) by use of interpolation subroutines (SPLINE and PCUBIC).[13] The constructed $G^2(t)$'s were analyzed by the same program as that used in the analysis of experimental $G^2(t)$'s, yielding simulated D_{app} versus K relationships.

The value of $D_{[n]} = (k_BT/\zeta L)$ in eq 10 and $D° = (k_BT/3\pi\eta L)$ in eq 14 can be estimated from eqs 13 and 15 (with $\sigma = 1/2$, or $\zeta = 3\pi\eta$ by analogy to a string of touching spherical beads) for the experimental D value of 3.60 and a given γL value; i.e.

$$D_{[n]} = D° = D(\text{obsd})/(1 + f_0)$$

By substituting this $D_{[n]}$ into eq 10 and $D°$ into eq 13, the D_{app} versus K relationship was simulated for γL = 30 and L = 900 nm (label a in Figure 2). This free-draining limit (for $D_{[n]}$) of the D_{app} versus K relationship shows much smaller D_{app} values than the observed ones (circles in Figure 2). When $D_{[n]}$ in eq 9 is replaced with D(obsd), the simulated D_{app} versus K relationship (label c in Figure 2) shows much larger D_{app} values than the observed ones. These preliminary simulations suggest the importance of the hydrodynamic interaction on the internal modes of motion; $D_{[n]}$ in eq 10 should depend on the mode number n, and $D° < D_{[n]} < D$.

3. Effect of Hydrodynamic Interaction on $g^1(t)$. The consideration in this subsection follows our previous perturbation method for a semiflexible rod.[14] In the framework of the Zimm model,[15] it is easily shown that eq 7 with eqs 4 and 8 is highly valid provided that $D_{[n]}$ in eq 10 is replaced with

$$D_{[n]} = D°[1 + f_n] \tag{16}$$

where $D°$ is given by eq 14. As in ref 15, a form of $f(|s - s'|) = \sigma(6/\pi)^{1/2}(\gamma/|s - s'|)^{1/2}$ (for a continuous chain model) is assumed for the preaveraged hydrodynamic interaction without the excluded volume effect, yielding f_0 in eq 15 and

$$f_n = f_0(9/8)^{1/2}(1/\pi n)^2\lambda'_n \tag{17}$$

where the eigenvalues, λ'_n, have been tabulated.[16] If we put $D° = D(\text{obsd})/(1 + f_0)$ for $\sigma = 1/2$ as before, we have

$$D_{[n]}/D(\text{obsd}) = (1 + f_n)/(1 + f_0) = r_n \tag{18}$$

where f_n can be computed by referring to the tabulated values of λ'_n (for $n > 7$, the asymptotic formula (eq 8 in ref 15) may be used). When the hydrodynamic interaction is taken into account in this way, the simulated D_{app} versus K relationship (label b-1 in Figure 2) becomes close to the observed one. In the framework of the present theory, $D°$ in both eqs 10 and 16 should be equal to $(k_BT/3\pi\eta L)$. However, eq 2 (or eq 13 with $\sigma = 1/2$) gives D = 3.90 for L = 900 nm and γL = 30, which is larger by 0.30 units than the observed D value of 3.60. Then when $D°$ in eq 13 was put equal to D(obsd)/$(1 + f_0)$ for D_{app} at K = 0 to be 3.60 but $D°$ in eq 16 to $(k_BT/3\pi\eta L)$, we have the simulated result shown in Figure 2 (label b-2). The curve with label b-2 is a little bit steeper at large K than the curve with label b-1. This is due to the fact that the latter $D°$ is larger than the former $D°$.

Theoretically speaking, the input parameters for computation of $g^1(t)$ are L and γL, or $\langle R^2\rangle$ and γL. In our simulation of the D_{app} versus K relationship in Figure 2, the input parameters were D(obsd), γL, and L. In this case, D(obsd) was used to determine the $D°$ value, and $\langle R^2\rangle$ was automatically determined by eq 1. Then simulation of the D_{app} versus K relationship for various combinations of L and γL gives the best estimate of $\langle R^2\rangle$ through the analysis of the contributions to D_{app} from the internal modes of motion. It should be noted here that eq 18 is very insensitive to the γL values; for example, r_1 (r_2) = 0.517 (0.440), 0.495 (0.415), 0.485 (0.403), and 0.479 (0.396) for γL = 10, 20, 30, and 40, respectively, whereas $\langle R^2\rangle$ and hence x are roughly proportional to the inverse of γL (note $\langle R^2\rangle \sim L^2/(\gamma L)$ for large γL). Therefore, we can also simulate the D_{app} versus K relationship for given values of D(obsd), $\langle R^2\rangle$, and γL, where the γL value is rather arbitrary; a rough estimate of γL = 25–30 from D(Kirkwood) = D(obsd) may successfully be used. Figure 1 depicts the simulated results for given values of D(obsd), $\langle R^2\rangle$, and γL (=30).

4. Some Remarks. The Kirkwood formula for $\gamma L \gg 1$ gives $R_g/R_s = (8/3\,\pi^{1/2}) = 1.50$, the size of this ratio for Gaussian coils, where $R_g = (\langle R^2\rangle/6)^{1/2}$ is the root-mean-square radius of gyration and $R_s = (k_BT/6\pi\eta D)$ is the Stokes radius. We have $R_g/R_s = 1.51$ for $\langle R^2\rangle = 2.66 = (163\text{ nm})^2$ and D = 3.60. Although this excellent agreement of R_g/R_s is perhaps somewhat fortuitous, it strongly suggests that connectin is in a Gaussian coil conformation. Since estimation of R_g from $\langle R^2\rangle$ depends on the model (coil or rod) whereas that of R_s from D(obsd) does not, the ratio of 1.51 ensures our analyses of the I versus K and D_{app} versus K relationships based on formulas for Gaussian coils.

The overlap concentration is estimated to be $c^* = (M/N_AR_g^3) = 1.7$ mg/mL, where M is the molecular mass (3×10^6 Da) and N_A is the Avogadro number. Therefore, c/c^* for the present concentration of c = 0.2–0.8 mg/mL is not much smaller than unity, but the theoretical formulation for the dilute regime ($c/c^* \ll 1$) may be applicable in the analysis of experimental data.

In the non-free-draining limit ($h \gg 1$, where $h = \sigma(3/\pi)^{1/2}(\gamma L)^{1/2}$ in our wormlike chain model), we have approximations $f_0 \gg 1$ and $f_n \gg 1$, and hence D(Kirkwood) = $D°f_0 = (1/2)(6/\pi)^{1/2}(8/3)(k_BT/3\pi\eta)\langle R^2\rangle^{-1/2}$ and $D_{[n]} = D°f_n = D°f_0(9/8)^{1/2}(1/\pi n)^2\lambda'_n$. Then the Langevin relaxation time in eq 9 can be rewritten as $\tau_n = (\pi/2)(\pi/3)^{1/2}(\eta\langle R^2\rangle^{3/2}/k_BT\lambda'_n)$. In the same limit, the viscoelastic relaxation time has been given as $\tau'_n = (\pi/4)(\pi/3)^{1/2}(\eta\langle R^2\rangle^{3/2}/k_BT\lambda'_n)$ (see eqs 81–83 of ref 15). Then we have the well-known relation $\tau_n = 2\tau'_n$, showing the correctness of f_n in eq 17. For $\langle R^2\rangle$ = 2.66, r_1 = 0.485 (γL = 30), and D(obsd) = 3.60, eq 9 gives τ_1 = 515 μs (and, roughly speaking, $\tau_2 \sim 130$ μs and $\tau_3 \sim 60$ μs). This Langevin

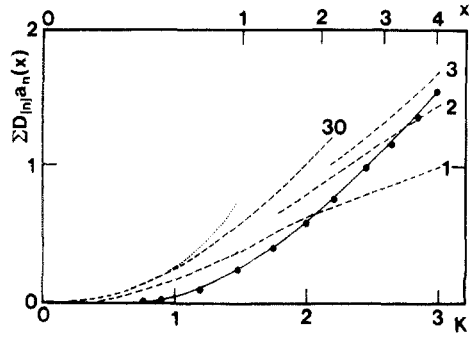

Figure 3. Contributions to D_{app} from the internal modes of motion. Filled circles show observed values of $D_{app} - D$ (taken from Figure 1), and the solid line is merely a visual guide. Broken lines show computed results of $\Sigma' D_{[n]}a_n(x)$ in eq 11 at 10 °C for $\langle R^2 \rangle = 2.66$, $\gamma L = 30$, and $n_{max} = 1$, 2, 3, and 30 for labels 1, 2, 3, and 30, respectively. The dotted line shows $D_{app} - D = DCx$ with $C = 0.14$ and $D = D(\text{obsd})$.

relaxation time of $\tau_1 \sim 520$ μs can be compared with the viscoelastic relaxation time of $\tau'_1 \sim 290$ μs for $\langle R^2 \rangle = 2.66$ and $\eta = 1.31$ cP at 10 °C. We observe a difference of ca. 10% between τ_1 (from eq 9) and $2\tau'_1$. This difference mostly comes from the approximations $f_0 \gg 1$ and $f_n \gg 1$, which are not highly valid in our particular case of $\gamma L = 25$–30. Thus, we adopt Hearst's expression for the intrinsic viscostiy,[17] $[\eta] = 2.81 \times 10^{23}(\langle R^2 \rangle^{3/2}/M)h'F(h')$, with $h' = 2h = 2\sigma(3\gamma L/\pi)^{1/2}$, which gives $[\eta] = 280$ mL/g for $\langle R^2 \rangle = 2.66$, $\gamma L = 30$, and $M = 3 \times 10^6$ Da. (Zimm's formula is given by putting $h'F(h') = 1$ for $h' \gg 1$,[15] which gives $[\eta] = 410$ mL/g.) On the other hand, the literature value of $[\eta]$ for connectin is ca. 180 mL/g (obtained with an Ostwald type viscometer with a mean velocity gradient of 500 s^{-1}).[8] Since we did not measure $[\eta]$ of our own sample, we do not have any definite idea about the difference between these two values. However, we have to be satisifed with this rough agreement, particularly in view of the fact that the measurement of $[\eta]$ in the literature was not originally designed for this kind of critical cross-comparison.

The spatial ranges in our study are characterized by the following two inequalities, $0.5 \leq KR_g \leq 2$ and $0.2 \leq K\gamma^{-1}$ $(=Kb) \leq 1$ ($\gamma^{-1} = 30$ nm for $\gamma L = 30$ and $L = 900$ nm). Thus, our situation is neither in the small-K region ($KR_g \ll 1$) nor in the large-K region ($Kb \gg 1$). Also, it is not in the so-called intermediate-K region ($KR_g \gg 1$ *and* $Kb \ll 1$). In our particular situation, therefore, the numerical method described above may be the simplest of those feasible for the analysis of DLS spectra.

5. On the Internal Modes. The contribution to D_{app} from the internal modes of motion, $\Sigma' D_{[n]}a_n(x)$ in eq 11, was experimentally estimated as shown by circles in Figure 3. The broken lines in Figure 3 show the computed values of $\Sigma' D_{[n]}a_n(x)$ for $\langle R^2 \rangle = 2.66$ and $\gamma L = 30$, where n_{max} in the summation was 1, 2, 3, and 30 (the same as labels attached to the broken lines). These numerical results suggest the following two points, at least.

Low-K Behavior of D_{app}. It has been theoretically discussed that the factor C in $D_{app} = D(1 + Cx + ...)$ for Gaussian coils has values of $^2/_{15} = 0.1333$ and $^{13}/_{75} = 0.1733$ for pre- and nonpreaveraged approximations, respectively.[18] It is easy to show $a_n(x) = 2x/(\pi n)^2 + ...$ (eq 12), so that $(1/D)\Sigma' D_{[n]}a_n(x)$, in our preaveraged approximation, and $D^\circ = D(\text{obsd})/(1 + f_0)$ give $C = 0.138$, 0.140, and 0.140 for $n_{max} = 10$, 20, and 30 (cutoff for $\gamma L = 30$), respectively. The dotted curve in Figure 3 shows $D_{app} - D = DCx$ for $C = 0.140$ and $D = D(\text{obsd})$. A difference of ca. 5% between $C = 0.140$ and 0.1333 is unimportant for our point that both experimental and simulated D_{app} versus K relationships at $K < 1$ gave a negligibly small C value. Let us rewrite eq 5 in the form

$$g^1(t) = \exp(-DK^2t)[P_0(x) + P_{int}(x,t)]/P(x)$$

where $P_0(x) = S(K,\infty) = (\pi/x)\exp(-x/6)[\text{erf}(x^{1/2}/2)]^2$,[9] and $P_{int}(x,t)$ $[=S(K,t) - P_0(x)]$ is the contribution from the internal modes of motion. Since $S(K,0) = P(x)$ as mentioned before, we can easily observe how $P_{int}(x,0) = x^2/45 + ...$ is small compared with $P(x)$ and $P_0(x)$ at $x < 1$; $P_{int}(x,0)/P_0(x) = 0.0043$ at $x = 0.44$ ($K = 1$) and 0.021 at $x = 1$. (The sizes of $P(x)$, $P_0(x)$, and $P_{int}(x,0)$ for x in the range [1, 7] have been given graphically; note that $P_{int}(x,0)$ is the sum of P_2 and P_s in that figure.[9]) Therefore, the cumulant expansion method would give $D_{app} \sim D$ for $x < 0.44$ ($K < 1$) even if $D_{[n]}a_n(x)$'s for small n have appreciable values.

Number of Internal Modes. The numerical results in Figure 3 suggest that important contributions to D_{app} arise from internal modes with n up to 3 at the most. This situation is qualitatively understood as follows. The relaxation time of the nth mode of motion is given by $\tau_n = 2x/(\pi nK)^2 D_{[n]}$ (see eqs 4 and 9). From the Einstein relation, the mean-square amplitude of the nth mode is given by $\langle A_n^2 \rangle = 6D_{[n]}\tau_n = 12x/(\pi nK)^2$, or $\langle A_n^2 \rangle K^2 = 12x/(\pi n)^2$. A "spatial" condition for which the nth mode is detected will be $\langle A_n^2 \rangle K^2 > 1$,[19] or $x > (\pi n)^2/12$ (this condition for $n = 1$ is equivalent to a conventional condition of $KR_g > 1$). As shown before (see eq 18), we have $D_{[n]} \sim D/2$ (for $n = 1$ and 2), or $\tau_n \sim 4x/(\pi^2 n^2 DK^2)$. In measuring $G^2(t)$, we usually set $DK^2 t_{max} = 2$ with $t_{max} = 256t_s$ (t_s = the sampling time). For the nth mode to be detected, a "temporal" condition will be $\tau_n/t_s > 20$ (the nth mode should contribute to $g^1(t)$ up to the first 20 bins, at least, out of total 256), or $x > (\pi n)^2/25$. That is both spatial and temporal considerations suggest a condition $x > (0.4\text{–}0.8)n^2$ for the internal motions up to the nth mode to be detected experimentally. Another view,[12] but equivalent to the above one, is that both eq 11 and the above cited $D_{app} = D[1 + Cx + ...]$ were derived from the time derivative of $g^1(t)$ at $t = 0$, whereas from an experimental point of view, D_{app} should be derived from the time derivative of $g^1(t)$ at $t = t_s$, at least. Instead of eq 11 we then have $D_{app} = D + \Sigma' D_{[n]} \exp(-t_s/\tau_n)a_n(x,t_s)$. If $\tau_1/t_s = 20$ is assumed for example, then we have $\Sigma' \exp(-t_s/\tau_n) \sim \Sigma' \exp(-n^2/20) = 3.5$; that is, the effective n_{max} of 3.5 is very much smaller than $n_{max} = 30$ (cutoff value for $\gamma L = 30$).

6. γL Dependence of D_{app} for a Monodisperse Distribution. When $\langle R^2 \rangle$ and γL are adopted as the input parameters for computation of $g^1(t)$, the contour length L is not required as mentioned before. To examine possible effects of sample polydispersity, however, L and γL are adopted in what follows. From an electron microscopic observation with a very clever technique for specimen preparations, the length distribution of connectin molecules has been reported.[4] The distribution of the TII_B fraction of connectin is very sharp (the length distribution is sketched in Figure 5), given below), the contour lengths ranging from 800 to 1000 nm with the number-average length $L_n = (904 \pm 50)$ nm, the weight-average length $L_w = (908 \pm 60)$ nm, and $L_w/L_n = 1.004$. Since we did not measure the length distribution of our own samples, we first assumed a monodisperse situation.

Case A. Since the experimental D value of 3.60 and the assumed L values of 900 and 800 nm were given as input parameters, only the γL value was left as adjustable. By putting $D^\circ = D(\text{obsd})/(1 + f_0)$ in eqs 13 and 16 as before, the simulated D_{app} versus K relationships were obtained

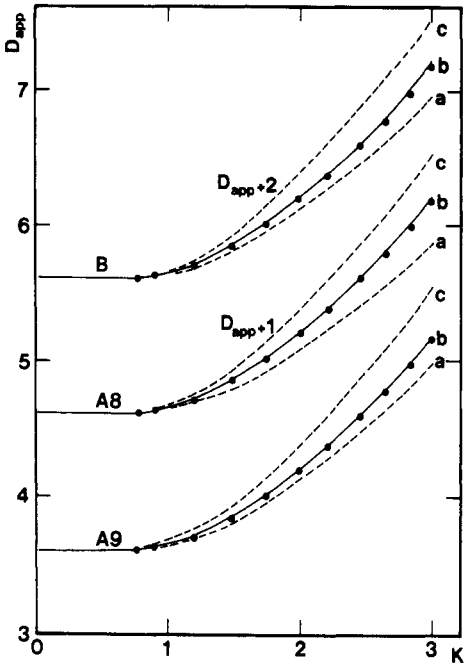

Figure 4. Simulated D_{app} versus K relationships at 10 °C. Monodisperse situation. Label A9 denotes case A for L = 900 nm; γL values were 35 for label a, 30 for label b, and 25 for label c. Label A8 denotes case A for L = 800 nm (D_{app}'s are displyed with a shift by one unit); γL values were 30 for label a, 23.5 for label b, and 20 for label c. Label B denotes case B for L = 900 nm (D_{app}'s are displayed with a shift by two units), γL values were 35 for label a, 30 for label b, and 25 for label c. See text for definition of cases A and B. Filled circles were taken from Figure 1.

as shown in Figure 4 (labels A9 and A8). The observed D_{app} versus K relationship was close to the simulated ones for L = 900 nm and γL = 30, or $\langle R^2 \rangle$ = 2.66 = (163 nm)^2, and for L = 800 nm and γL = 23.5, or $\langle R^2 \rangle$ = 2.67 (=163 nm)^2. As expected, the absolute value of the contour length is not important to estimate $\langle R^2 \rangle$. From $D^\circ = (k_B T/3\pi\eta L)$, eqs 13 and 15 (with $\sigma = {}^1/_2$), the Kirkwood D values at T = 10 °C were calculated to be 3.90 (for γL = 30 and L = 900 nm) and 3.93 (for γL = 23.5 and L = 800 nm). These D values were close to, but 8% larger than, the observed one. Then the following two alternative simulations were made.

Case B. The σ value was calculated from D(Kirkwood) = D(obsd):

$$\sigma = [D(\text{obsd})/(k_B T/3\pi\eta L) - 1]/3.685(\gamma L)^{1/2}$$

This way of adjusting the size of σ apparently corresponds to adjusting the size of the draining parameter h and/or taking the excluded volume effect into account; $D = D^\circ[1 + f_0(1 - 0.609z + ...)]$.[20] For L = 900 nm and T = 10 °C we have σ = 0.500 (γL = 25), 0.456 (γL = 30), and 0.423 (γL = 35). In this case, both the Kirkwood D value and $D_{[n]}$ in eq 9 were independent of γL values, but $\langle R^2 \rangle$ and hence τ_n were not. Simulated results for adjusted σ values are also shown in Figure 4 (label B), which were virtually the same as those for $\sigma = {}^1/_2$ (label A9).

Case C. An effective value of L in D° of eq 14 was determined by putting D(Kirkwood) = D(obsd) for $\sigma = {}^1/_2$ and a given γL; for example, L = 900, 976, 1100, and 1710 nm for γL = 25, 30, 40, and 100, respectively. The simulated results (not shown) for these L and γL values were found to be very insensitive to the γL values and did not come close to the observed result for a reasonable range of effective L values. The above L and γL give $\langle R^2 \rangle$ = 3.17, 3.12, 2.99, and 2.88 for γL = 25, 30, 40, and 100, respectively. Thus, $\langle R^2 \rangle$ decreases very slowly with γL. This is the sole reason why the D_{app} versus K relationship was very weakly dependent on γL values in this case.

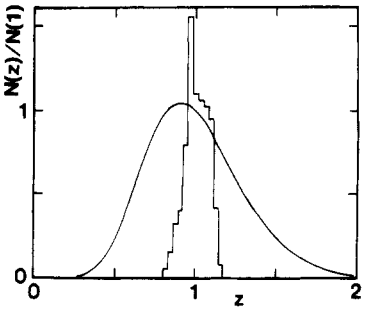

Figure 5. Length distribution $N(z)$ for connectin as a function of $z = L/L_n$. The histogram shows $N(z)$ for the TII_B fraction of connectin (a very rough sketch of Figure 5d in ref 4). The solid line shows the Schulz–Zimm function for m = 10, where appreciable fractions of filaments with lengths shorter than $0.5L_n$ and longer than $1.5L_n$ are observed; $z_n = 1.00 \pm 0.30$ and $z_w = 1.09 \pm 0.31$. (Referring to the description in ref 4 for their electron microscopic observation of β-connectin, we assumed m = 10 as the worst value of the polydispersity parameter.)

7. γL Dependence of D_{app} for a Polydisperse Distribution. To see the possible effects of a length distribution of connectin filaments on the D_{app} versus K relationship, the Schulz–Zimm distribution function without the normalization constant is assumed:[7]

$$N(z) = z^m \exp[-(m+1)z]$$

where $N(z)$ is defined as the "number" of filaments with length $z = L/L_n$ and m is the parameter determining the width of the distribution. For this distribution, we have $L_w/L_n = (m+2)/(m+1)$. The distribution $N(z)$ for m = 10 is depicted in Figure 5. The average of $g^1(t)$ over the length distribution is given by

$$\langle g^1(t) \rangle = \int g^1(z,t) z^2 N(z)\, dz / \int z^2 N(z)\, dz \qquad (19)$$

$$g^1(z,t) = \exp[-D(z)K^2 t] S(z,t)/S(z,0) \qquad (20)$$

where $S(z,t)$ is given by eq 6 for $L = L_n z$ and

$$D(z) = D^\circ(z)[1 + f_0(z)] \qquad (21)$$

$$D^\circ(z) = (k_B T/3\pi\eta L_n z) \qquad (22)$$

$$f_0(z) = 3.685(\gamma L_n z)^{1/2}\sigma \qquad (23)$$

The mean-square end-to-end distance, $\langle R^2 \rangle$, for length z, is given by eq 1 with $L = L_n z$. Equation 16 should be replaced with

$$D_{[n]} = D^\circ(z)[1 + f_0(z)(9/8)^{1/2}(1/\pi n)^2 \lambda'_n] \qquad (24)$$

From eqs 21–23, the light scattering D value ($\langle D_{app} \rangle$ value at K = 0) is given by $\langle D(z) \rangle = (k_B T/3\pi\eta L_n)[\langle 1/z \rangle + 3.685(\gamma L_n)^{1/2}\langle (1/z)^{1/2} \rangle \sigma]$, where $\langle g(z) \rangle = \int g(z) z^2 N(z)\, dz / \int z^2 N(z)\, dz$. It is easy to show $\langle 1/z \rangle = L_n/L_w$ and $\langle (1/z)^{1/2} \rangle \sim (L_n/L_w)^{1/2}$ for large m (99% correct for m = 10). Then we have

$$\langle D(z) \rangle = \langle D^\circ(z) \rangle [1 + 3.685(\gamma L_w)^{1/2}\sigma] \quad (m \geq 10) \qquad (25)$$

$$\langle D^\circ(z) \rangle = (k_B T/3\pi\eta L_w) \qquad (26)$$

The z average of D, $\langle D(z) \rangle$, is given by the Kirkwood formula with $L = L_w$.

The integration over z in eq 19 was replaced with summation over 12 evenly spaced points from $L_n A$ to $L_n B$ where A (<1) and B (>1) satisfied $N(A) = N(B) = 0.01N(1)$. Corresponding to cases A and B for a monodisperse

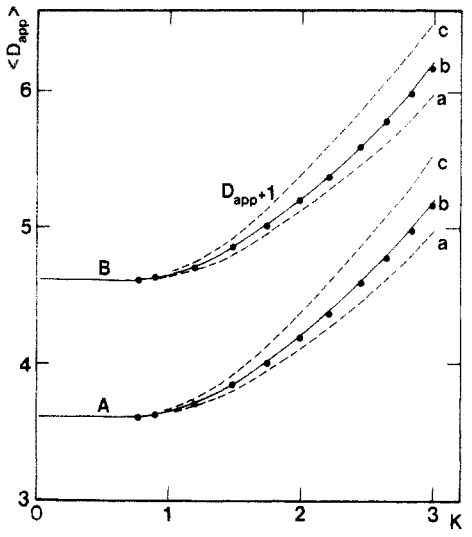

Figure 6. Simulated $\langle D_{app} \rangle$ versus K relationships at 10 °C. Polydisperse situation with $m = 10$. Labels A and B denote cases A and B for $L_w = 900$ nm ($\langle D_{app} \rangle$'s for case B are displayed with a shift by one unit); $\gamma L_w = 35$ for label a, 30 for label b, and 25 for label c. Filled circles were taken from Figure 1.

distribution discussed above, the following two cases were computed for eq 19.

Case A. Referring to eqs 25 and 26, we put

$$D^\circ(z) = \langle D^\circ(z) \rangle (L_w/L_n z) \tag{22'}$$

$$\langle D^\circ(z) \rangle = D(\text{obsd})/[1 + 1.84(\gamma L_w)^{1/2}] \tag{26'}$$

Then eq 21 with eqs 23 (for $\sigma = {}^1/_2$), 22' and 26' gives $\langle D_{app} \rangle = D(\text{obsd})$ at $K = 0$. By using eq 24 with eqs 22' and 26', the $\langle D_{app} \rangle$ versus K relationships were simulated for $L_w = 900$ nm (label A in Figure 6). From $L_w = 900$ nm and $\gamma L_w = 30$, we have $\langle R^2 \rangle_w = 2L_w^2(2\gamma L_w - 1)/(2\gamma L_w)^2 = 2.66$ (=163 nm)^2.

Case B. If we put

$$\sigma = [D(\text{obsd})/(k_B T/3\pi\eta L_w) - 1]/3.685(\gamma L_w)^{1/2}$$

then eq 21 with eqs 22 and 23 gives $\langle D_{app} \rangle = D(\text{obsd})$ at $K = 0$. The simulated $\langle D_{app} \rangle$ versus K relationships are shown in Figure 6 (label B) for $L_w = 900$ nm. Again, the best fit curve was obtained for $\gamma L_w = 30$.

8. Average of $P(x)$ over the Size Distribution. For simplicity of algebra, we use an approximate form of $\langle R^2 \rangle = L/\gamma = (L_n z/\gamma) = [(m + 1)/(m + 2)](L_w z/\gamma) = [(m + 1)/(m + 2)]\langle R^2 \rangle_w z$. Then the average of $P(x)$ over the size distribution is given by

$$\langle P(x) \rangle = (2/x_w^2)[(m + 2)/(m + 1)]\{[1 + x_w/(m + 2)]^{-(m+1)} - 1 + [(m + 1)/(m + 2)]x_w\} \tag{27}$$

where $x_w = K^2\langle R^2 \rangle_w/6$. (For small x_w the above equation gives $\langle P(x) \rangle = 1 - x_z/3 + \ldots$ (with $x_z = K^2\langle R^2 \rangle_z/6$) as it should be, where use was made of $[(m + 3)/(m + 2)]\langle R^2 \rangle_w = L_z/\gamma = \langle R^2 \rangle_z$). When the I versus K relationship is fitted with $I(K) = k_s\langle P(x) \rangle$ as before, we can find $\langle R^2 \rangle_w = 2.55$–$2.65$ ($m = 10$).

9. Concluding Remarks. We have described, in some detail, the analysis of the DLS spectra for isolated connectin filaments in solution in terms of a wormlike chain model with a preaveraged hydrodynamic interaction. The result of the analysis gave the mean-square end-to-end distance $\langle R^2 \rangle = (163 \text{ nm})^2$ and the number $\gamma L = 30$ and length $\gamma^{-1} = 30$ nm of the Kuhn statistical segments for the contour length $L = 900$ nm. The statistical segment length of connectin filaments is an order of magnitude shorter than those of an α-helical polypeptide, poly(γ-benzyl L-glutamate) in dimethylformamide ($\gamma^{-1} = 313$ nm)[21] and of collagen ($\gamma^{-1} = 340$ nm).[22] This high flexibility of connectin is compatible with the fact that that molecule does not contain any α-helical structure but consists of a random coil and β-sheet structure.[2] Details of the experimental part of this study, estimation of elastic moduli such as the flexural rigidity, the Young's modulus, and the elastic constant for extension of the contour length L, and implications of these results in muscle physiology will be given elsewhere.[5]

Acknowledgment. We thank Professor K. Maruyama and Mr. Y. Nakauchi of Chiba University for their collaboration in the experimental part of this study.

References and Notes

(1) Visiting scientist from the Jikei University School of Medicine, Tokyo. Present address: Yanagida Biomotron Project, Exploratory Research for Advanced Technology, Research Development Corporation of Japan, 2-4-14 Semba-higashi, Mino, Osaka 562, Japan.
(2) Maruyama, K. *Int. Rev. Cytol.* **1986**, *104*, 81.
(3) Wang, K. *Cell and Muscle Motility*; Shay, J. W., Ed.; Plenum Publishing: New York, 1985; Vol. 6, pp 315–369.
(4) Nave, R.; Furst, D. O.; Weber, K. *J. Cell Biol.* **1989**, *109*, 2177.
(5) Higuchi, H.; Nakauchi, Y.; Maruyama, K.; Fujime, S. *Biophys. J.* **1993**, in press.
(6) To avoid confusion, note that when the words "Gaussian coil" are used for connectin, they mean that the overall shape (or quaternary structure) of a single connectin filament assumes a Gaussian coil; they never mean a random coil conformation in the secondary structure of connectin.
(7) Yamakawa, H. *Modern Theory of Polymer Solutions*; Harper and Row: New York, 1971.
(8) Maruyama, K.; Kimura, S.; Yoshidomi, H.; Sawada, H.; Kikuchi, M. *J. Biochem. (Tokyo)* **1984**, *95*, 1423.
(9) Pecora, R. *J. Chem. Phys.* **1968**, *49*, 1562.
(10) Fujime, S. *J. Phys. Soc. Jpn.* **1970**, *29*, 751.
(11) Fujime, S.; Maruyama, M. *Macromolecules* **1973**, *6*, 237.
(12) Maeda, T.; Fujime, S. *Macromolecules* **1980**, *14*, 809.
(13) Maeda, T.; Fujime, S. *Macromolecules* **1985**, *18*, 2430.
(14) Fujime, S.; Maeda, T. *Macromolecules* **1985**, *18*, 191.
(15) Zimm, B. H. *J. Chem. Phys.* **1956**, *24*, 269.
(16) Zimm, B. H.; Roe, M.; Epstein, L. F. *J. Chem. Phys.* **1956**, *24*, 279.
(17) Hearst, J. E. *J. Chem. Phys.* **1962**, *37*, 2547.
(18) Burchard, W.; Schmidt, M.; Stockmayer, W. H. *Macromolecules* **1980**, *13*, 580.
(19) Fujime, S. *J. Phys. Soc. Jpn.* **1971**, *31*, 1805.
(20) Stockmayer, W. H.; Albrecht, A. C. *J. Polym. Sci.* **1958**, *32*, 215.
(21) Kubota, K.; Tominaga, Y.; Fujime, S. *Macromolecules* **1986**, *19*, 1604.
(22) Kubota, K.; Tominaga, Y.; Fujime, S. *Biopolymers* **1987**, *26*, 1717.